recycling

MDPI

Article

End-of-Life Tire Geocells for Unpaved Road Reinforcement: A Comparative Performance Assessment Under Cyclic Loading

María Paula Susunaga [1,*], Ennio Marques Palmeira [2], Ivonne Alejandra Gutiérrez Góngora [3], Karla Yolima Rodriguez Rodríguez [1] and Juan Sebastián Perdomo Díaz [1]

[1] Department of Civil Engineering, Engineering Faculty, University of Ibagué, Ibague 730001, Colombia; 2520211051@estudiantesunibague.edu.co (K.Y.R.R.); 2120211016@estudiantesunibague.edu.co (J.S.P.D.)
[2] Department of Civil and Environmental Engineering, University of Brasília, Federal District, Brasilia 70910-900, DF, Brazil; palmeira@unb.br
[3] Department of Civil Engineering, Catholic University of Brasília, Brasilia 71966-700, DF, Brazil; ivonne.gongora@ucb.br
* Correspondence: maria.salazar@unibague.edu.co

Abstract

The growing generation of end-of-life tires and the structural deficiencies of tertiary road networks in developing regions represent two interconnected challenges that call for integrated engineering solutions. Although recycled tire geocells have been explored as a reinforcement alternative for unpaved roads, their mechanical performance has not been systematically compared against conventional high-density polyethylene (HDPE) geocells under controlled cyclic loading, nor has the material valorization potential been quantified in terms of waste diversion capacity. This study systematically evaluates and compares the deformation response, stress distribution, and aggregate degradation of both systems through large-scale laboratory testing. An instrumented steel chamber was used to apply up to 100,000 load cycles at 600 kPa contact pressure, across two cell heights (150 mm and 200 mm) and two granular infill qualities. The 200 mm recycled tire geocell reduced permanent surface deformation by up to 84% relative to the unreinforced condition, and Traffic Benefit Ratio values reached up to 1.6 times those recorded for HDPE geocells under lower-quality infill. The viscoelastic response of rubber promoted energy dissipation and limited aggregate particle breakage. Confinement performance was fully preserved after surface reconditioning, confirming the durability of the reinforcement system under maintenance cycles. The fabrication process requires no chemical transformation, valorizing approximately 16 end-of-life tires per square meter—equivalent to 56,000 tires per kilometer of reinforced road. These findings support the large-scale valorization of end-of-life tires as functional geotechnical materials, offering a circular economy pathway for solid waste diversion in regions where both road infrastructure deficits and tire disposal challenges coexist.

Keywords: end-of-life tires; circular economy; waste valorization; low-volume roads; cyclic loading; sustainable geosynthetics

Check for updates

Academic Editor: Sébastien M. R. Dente

Received: 29 May 2026
Revised: 3 July 2026
Accepted: 7 July 2026
Published: 20 July 2026

Copyright: © 2026 by the authors. Licensee MDPI, Basel, Switzerland. This article is an open access article distributed under the terms and conditions of the Creative Commons Attribution (CC BY) license.

1. Introduction

The performance and longevity of transportation infrastructure depend critically on the mechanical behavior of granular layers under repeated traffic loading. In low-volume road networks, where unpaved surfaces are prevalent, the absence of adequate subgrade reinforcement leads to accelerated deterioration, high maintenance costs, and reduced

accessibility, particularly in developing regions. The incorporation of recycled materials into such infrastructure has opened a pathway for improving structural performance while reducing the environmental impacts associated with waste disposal and raw material extraction. In particular, the geotechnical engineering community has increasingly explored the valorization of industrial and post-consumer waste as engineering materials capable of replacing conventional resources [1,2]. Among the various waste streams generated worldwide, end-of-life tires represent one of the most challenging materials to manage due to their durability, complex composition, and limited recycling pathways. It is estimated that approximately 1.5 billion waste tires are generated globally every year, creating significant environmental challenges related to storage, fire hazards, and potential contamination when improperly managed [3,4]. Nevertheless, tire rubber possesses intrinsic mechanical characteristics such as high elasticity, fatigue resistance, and durability that make it a promising candidate for engineering applications. Consequently, transforming waste tires into geotechnical construction materials has emerged as a viable strategy to simultaneously address waste management challenges while developing functional materials for transportation infrastructure systems [5–7].

Recycled tire rubber exhibits mechanical and physical properties that are advantageous for several construction applications. Due to its elastomeric nature, rubber presents high flexibility, significant resistance to cyclic fatigue, and the ability to dissipate energy through damping mechanisms [4,7]. These characteristics have motivated its use in a variety of infrastructure materials, including rubberized asphalt mixtures, vibration isolation systems, and lightweight geomaterials [8,9]. In addition, the relatively low density and high resilience of recycled rubber particles allow the material to absorb stresses and reduce stress concentrations within granular matrices [10,11]. Previous studies have demonstrated that incorporating recycled rubber into construction systems can enhance durability and reduce aggregate degradation under repeated loading conditions [9]. Furthermore, the use of tire-derived materials in civil engineering applications has been widely investigated, demonstrating their potential as lightweight and resilient geomaterials in transportation infrastructure [12–14]. Overall, these properties, particularly the capacity for energy dissipation and stress redistribution under cyclic loading, suggest that recycled tire rubber may also perform effectively as the structural wall material in geocell confinement systems, where the reinforcement mechanism is strongly influenced by fatigue resistance and controlled deformability.

Geocells are three-dimensional cellular confinement systems widely used to improve the mechanical performance of granular layers in transportation infrastructure. When deployed on the subgrade and filled with granular materials, geocells provide lateral confinement that increases the stiffness, shear resistance, and load distribution capacity of the reinforced layer [15,16]. This confinement mechanism reduces lateral spreading of the infill material and limits permanent deformation under repeated traffic loading [17,18]. Experimental and numerical studies have demonstrated that geocell reinforcement significantly improves bearing capacity and reduces rutting in unpaved road systems and other geotechnical applications [19–21]. In addition, geocell-reinforced layers subjected to cyclic loading have shown improved structural stability and reduced permanent deformation compared with unreinforced granular systems [22].

The performance of geocell-reinforced systems depends not only on the cellular geometry but also on the mechanical properties of the material used to fabricate the cell walls. The confinement mechanism is governed by the interaction between the infill material and the geocell walls, where tensile stresses develop within the cell structure and mobilize lateral restraint against particle displacement [15,17]. Under repeated loading, this interaction enhances load distribution and reduces stress concentrations within the

granular matrix. Therefore, the stiffness, flexibility, and fatigue resistance of the cell wall material play a critical role in determining the overall structural response of the reinforced layer. Conventional geocells are typically manufactured from high-density polyethylene (HDPE), a polymer characterized by relatively high tensile strength and stiffness. However, the rigidity of HDPE may also promote localized stress concentrations within the aggregate under cyclic loading conditions. In contrast, recycled tire rubber exhibits greater deformability and energy dissipation capacity, which could potentially modify the confinement mechanism by redistributing stresses more uniformly within the granular matrix and reducing particle breakage. This potential advantage is particularly relevant in low-resource contexts where cost-effective and locally sourced reinforcement materials are essential for improving road infrastructure [23].

The need for locally available and sustainable reinforcement alternatives is particularly evident in unpaved road systems in developing regions, where poor road conditions remain widespread. In Colombia, for instance, the tertiary road network spans approximately 142,284 km, representing nearly 69% of the national road network, of which an estimated 40% is in poor condition, and only a small proportion has any form of pavement [24]. Similar infrastructure deficits are observed across Latin America, Sub-Saharan Africa, and Southeast Asia, where low-cost, locally sourced, and sustainable reinforcement materials are critically needed to improve road performance while minimizing construction costs and environmental impacts [25].

In recent years, several studies have explored the reuse of tire-derived materials in geotechnical and transportation applications, including the use of shredded tires, rubber chips, and rubber–soil mixtures as lightweight geomaterials or reinforcing inclusions [6,12–14]. More recently, geocells manufactured from recycled tire segments have been proposed as an alternative confinement system capable of utilizing the structural properties of tire rubber while simultaneously reducing waste disposal. Although these studies suggest that tire-derived materials may provide adequate structural performance, the available literature remains limited in terms of systematic experimental characterization of recycled rubber geocells. Despite these advances, limited research has systematically investigated the deformation response, load-bearing capacity, stress distribution, and particle breakage behavior of recycled tire geocells compared with commercial HDPE geocells under controlled large-scale cyclic loading while considering multiple granular fill materials and reinforcement geometries.

To address this gap, this study evaluates the mechanical performance of geocells manufactured from recycled tire rubber and compares their response with conventional HDPE geocells used as the reference confinement system. Large-scale cyclic loading tests were conducted using an instrumented chamber to simulate traffic loading conditions and to quantify deformation, stress distribution, and aggregate degradation under different reinforcement configurations. The experimental program systematically evaluates the effect of geocell height (150 mm and 200 mm), cell wall material (recycled tire rubber vs. commercial HDPE), and fill type (recebo and base-type granular material) on accumulated surface deformation, Traffic Benefit Ratio, particle breakage index, flexibility, and subgrade stress distribution. The results support the technical viability and potential use of recycled tire geocells for unpaved road reinforcement as a sustainable alternative, particularly in resource-limited settings.

2. Materials and Methods

This study adopted a large-scale experimental approach to evaluate the mechanical performance of unpaved roads reinforced with commercial geocells and geocells manufac-

tured from recycled tires as an end-of-life tire valorization strategy, under cyclic loading conditions representative of vehicular traffic [17,26].

The methodology was structured into three stages: (i) definition of the experimental program, including material characterization and the reinforcement configurations evaluated; (ii) execution of cyclic loading tests using an instrumented full-scale physical model; and (iii) performance analysis based on the breakage index (Bg), Traffic Benefit Ratio (TBR), and flexibility index (FI). Details of the loading system, instrumentation, and construction of the test sections are provided in the following subsections.

2.1. Experimental Program and Test Matrix

To ensure proper interpretation of the results, eight experimental configurations were defined based on the type and height of the geocell reinforcement, as well as the type of granular infill material. An unreinforced section (UNR) was used as the control condition. The complete experimental matrix is summarized in Table 1.

Table 1. Experimental matrix.

Section ID	Reinforcement Type	Geocell Material	Height (mm)	Infill Material	Description
UNR-BM	None	—	—	Base material (BM)	Unreinforced section (control)
UNR-RM	None	—	—	Recebo (RM)	Unreinforced section (control)
BMCG	Geocell	HDPE (commercial)	150	Base material (BM)	Reinforced with commercial geocell
RMCG	Geocell	HDPE (commercial)	150	Recebo (RM)	Reinforced with commercial geocell
BMRTG150	Geocell	Recycled tire	150	Base material (BM)	Reinforced with recycled tire geocell
RMRTG150	Geocell	Recycled tire	150	Recebo (RM)	Reinforced with recycled tire geocell
BMRTG200	Geocell	Recycled tire	200	Base material (BM)	Reinforced with recycled tire geocell (higher confinement)
RMRTG200	Geocell	Recycled tire	200	Recebo (RM)	Reinforced with recycled tire geocell (higher confinement)

The reinforced sections included a commercial HDPE geocell with a height of 150 mm (CG), and recycled tire geocells (RTG) with heights of 150 mm and 200 mm. Two types of granular materials were considered: base material (BM) and recebo (RM), allowing evaluation of the interaction between reinforcement system, infill properties, and confinement height.

All configurations were constructed and tested under identical compaction and cyclic loading conditions, ensuring consistency in boundary and loading conditions while varying the reinforcement type, geocell height, and granular infill material.

2.2. Materials Characterization

This section describes the materials used in the cyclic loading tests conducted within the test chamber. The experimental setup consisted of a 450 mm subgrade and a 300 mm structural layer. Two types of granular materials were employed: a base-quality material meeting Colombian standards (INVIAS) and a lower-quality material typically used in the region.

Material characterization was performed in accordance with INVÍAS standards. These national procedures are technically based on, and largely equivalent to, internationally recognized ASTM standards, which ensures that the laboratory results obtained for grain-size distribution, compaction, and index properties can be interpreted within a widely accepted geotechnical framework. In this context, the base-type material complies with the requirements commonly associated with international specifications. The recebo material, although not fully meeting such criteria, was characterized using the same standardized testing procedures to maintain consistency and allow a direct comparison within the experimental program. For the reinforcement phase, both commercial geocells and geocells manufactured from recycled tires were implemented. The following subsections present the description and physical characterization of the materials employed in this study.

2.2.1. Subgrade Materials

The soil used as the subgrade was collected from the northern area of Ibagué, within the premises of the University of Ibagué. This material is predominant in the region and was classified as a silty sand (SM) according to the Unified Soil Classification System (USCS). The physical properties of the subgrade material are summarized in Table 2.

Table 2. Properties of the material used as subgrade.

Property	Result
Classification according to USCS [27]	SM
Liquid Limit (wL) (%) [28]	36.90
Plastic Limit (wP) (%) [29]	26.20
Plasticity Index (PI) (%) [29]	10.70
Specific Gravity [30]	2.66
CBR (%) [31]	2.00
Dry Density (g/cm^3) [32]	1.50
Optimum Moisture Content (%)	25

2.2.2. Structural Layer Materials

For the granular base layer, two types of aggregates were used to evaluate the influence of the infill material within the geocells on the overall structural performance. These included a base-course material that meets current INVÍAS specifications and a locally sourced subbase material representative of the area. Both materials were characterized and compacted under equivalent conditions.

Base Type Material

The granular base material corresponds to a crushed aggregate that meets the current INVÍAS specifications for base course structural layers. Table 3 presents the physical properties of the material, which is classified as a well-graded silty gravel with a maximum dry density of 2.19 g/cm^3.

Table 3. Properties of the base type and recebo-type material.

Property	Result Base-Type Material	Result Recebo-Type Material
Classification according to USCS [33]	GM-GW	SW
Dry Density (g/cm^3) [34]	2.19	2.19

Table 3. *Cont.*

Property	Result Base-Type Material	Result Recebo-Type Material
CBR (%) [31]	111.54	30.00
Percentage of Clay Lumps (%) [35]	0.21	29.00
Los Angeles Abrasion (%) [36]	35.00	85.00
Optimum Moisture Content (%)	7	8

Material Recebo Type

The recebo material was classified as a well-graded sand (SW) according to the USCS. Table 3 presents the properties of the material. It is characterized by reaching a maximum dry density of 2.19 g/cm^3. This material is widely used due to its low cost and easy accessibility.

Figure 1 represents the particle size distribution curve of the materials used in the experimental sections, including the subgrade, base type, and recebo.

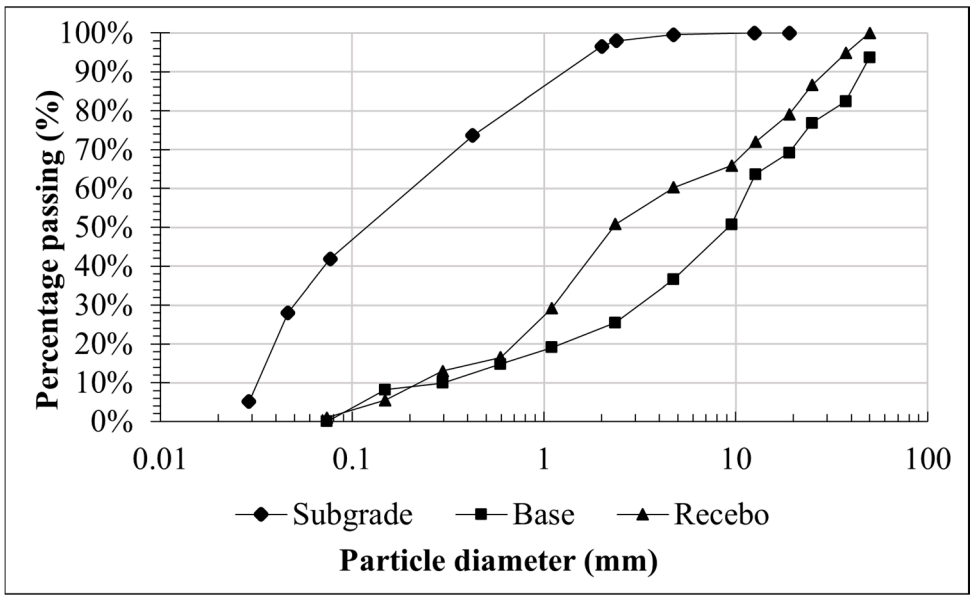


Figure 1. Particle size distribution of the subgrade, base type and recebo material.

2.2.3. Manufacturing Process of Recycled Tire Geocells

The manufacturing of geocells from recycled tires has been explored as a sustainable alternative for soil reinforcement by [6,37,38]. Among these studies, the one by [39], which has the patent NC 2017/0003522, stands out, documenting the systematic process for the construction and assembly of geocells. Although the exact procedure was not replicated in this study, its methodology served as a reference for designing the recycled tire geocells, ensuring consistency in geometry and mechanical behavior. Tires ranging from 13 to 20 inches in rim size were selected to maintain dimensional uniformity and structural compatibility among the manufactured units.

The manufacturing process was divided into four stages: (1) collection and storage of discarded tires from repair shops and service stations, stored under controlled conditions, (2) cutting and component rotation in which the sidewalls were removed, then inverted to enhance geometric regularity and ensure better fitting and uniformity, (3) assembly of modular units by joining the tread ends to form an eight-shaped ring, connected with industrial metal staples, and (4) formation of a three-dimensional mesh, which included

visual inspection, cleaning, and quality control to verify proper alignment, staple placement, and dimensional uniformity. This systematic approach ensured repeatability, durability, and mechanical stability in the final geocell structures.

Figure 2 represents the construction process of geocells made from tires.



Figure 2. Process of fabrication: (**a**) cutting of tire sidewalls, (**b**) rotation and preparation of tread components, (**c**) assembly of modular units and (**d**) formation of the three-dimensional mesh panels.

2.2.4. Physical Properties of the Geocells

The geocells used in this study were classified into two groups: a commercial high-density polyethylene (HDPE) geocell and two geocells manufactured from recycled tires. All reinforcements were employed as three-dimensional confinement systems to improve the mechanical response of granular layers under cyclic loading.

The commercial geocell, designated as CG, was manufactured from virgin HDPE and consisted of textured strips thermally fused at the weld points. In contrast, the recycled-tire geocells (RTG15 and RTG20) were fabricated from rubber tread sections obtained from discarded tires. These components were cut to nominal heights of 150 mm and 200 mm, respectively, and assembled using industrial metal staples to ensure structural continuity between adjacent cells as shown in Figure 2c. Table 4 summarizes the main physical properties of the three geocell configurations considered in the study.

Table 4. Physical properties of the geocells.

Property	Commercial Geocell	Recycled Tires with 150 mm Height	Recycled Tires with 200 mm Height
Material	Virgin HDPE	Rubber	Rubber
Cell height (mm)	150	150	200
Cell size (mm)	315 × 304	330 × 210	330 × 210
Connection type	Thermal fusion at weld points	Metal staples	Metal staples
Density (kg/m^3)	950	1100	1100

2.3. Experimental Setup and Loading Procedure

The experimental setup and loading procedure were designed to simulate the behavior of unpaved road sections under controlled cyclic loading conditions. This section describes the test assembly, instrumentation system, and loading protocol used to evaluate the mechanical response of the reinforced and unreinforced configurations.

2.3.1. Cyclic Loading Equipment and Protocol

The cyclic loading equipment used in the tests consists of a cylindrical steel chamber measuring 1200 mm in diameter and 1000 mm in height, equipped with three openings for the insertion and removal of materials. Its smooth, lubricated internal walls reduce friction with the soil, ensuring controlled testing conditions. The loading system comprises a hydraulic unit and an actuator, both regulated from a central panel that allows precise adjustment of the magnitude and frequency of the cyclic load, accurately simulating traffic-induced stresses on the road surface. Figure 3 shows the equipment used.

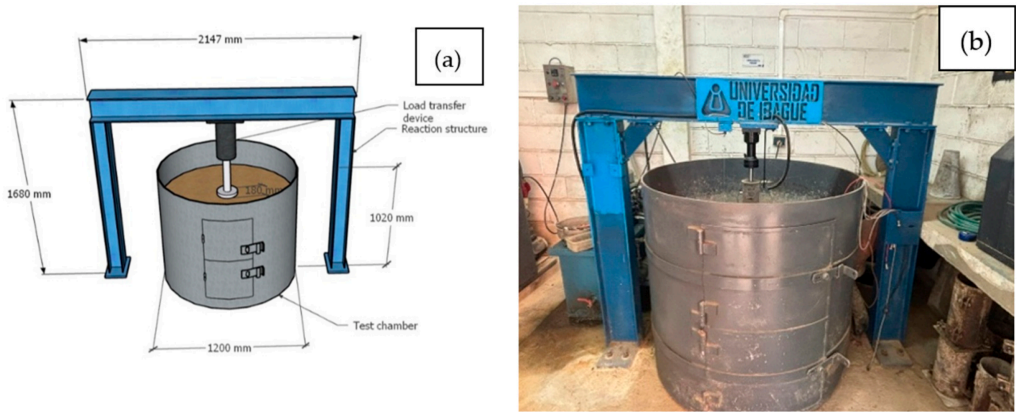


Figure 3. A schematic diagram (**a**) and photo (**b**) of the Cyclic loading equipment.

The loading protocol was designed to apply a maximum contact pressure of 600 kPa to the road section, corresponding to the estimated tire–surface contact pressure of a vehicle and consistent with values commonly used in physical model studies [40,41]. A frequency of 1 Hz was selected because it is widely used in resilient modulus testing and is consistent with the standard procedure reported in [42] allowing comparison with previous studies. The cyclic load was applied in a repeated pulsed waveform, reaching a maximum contact pressure of 600 kPa in each cycle, as illustrated in Figure 4. No seating load or preload was applied prior to the main cyclic loading stage.

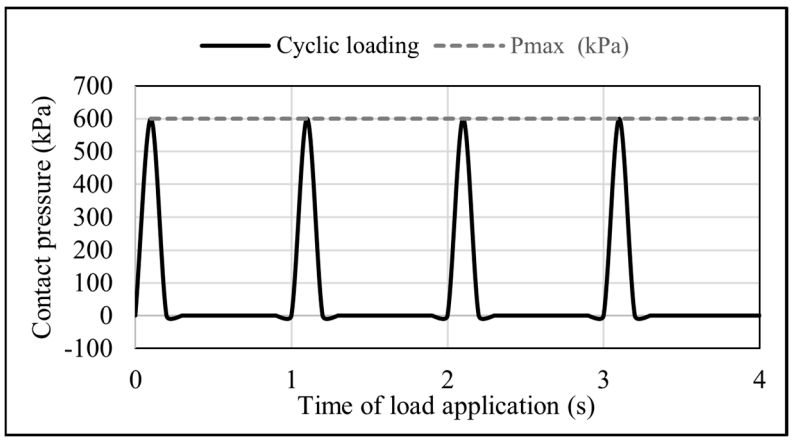


Figure 4. Frequency of the cyclic load.

The load was transmitted through a rigid circular plate with a diameter of 180 mm, which applied a constant maximum pressure throughout the test. The experiment was terminated when one of two predefined criteria was met: either a vertical deformation of 75 mm was reached, or 100,000 load cycles were completed, whichever occurred first.

Due to the complexity, duration, and resource demands of the large-scale cyclic loading setup, only one test was conducted for each configuration. Therefore, statistical measures of variability and error bars could not be reported. The results should be interpreted as exploratory and representative of the specific specimens tested, and the conclusions are limited to the mechanical response observed under the experimental conditions evaluated.

The internal diameter of the cylindrical chamber was set at 1200 mm, approximately six times larger than the loading plate (180 mm), to minimize boundary effects and ensure a more uniform stress distribution throughout the test section. This geometric ratio falls within the range adopted in previous large-scale cyclic loading studies aimed at evaluating the behavior of geosynthetic-reinforced granular layers. For instance, ref. [43] employed a chamber roughly five times larger than the loading plate, while [44] used a ratio of about four. Therefore, the experimental setup developed in this research remains consistent with configurations widely reported in the literature, ensuring the comparability and validity of the obtained results.

2.3.2. Instrumentation

An instrumentation system composed of stress, displacement, and load sensors was implemented to collect simultaneous data during the application of cyclic loads on the soil. The total stress cells, specifically developed for this research, were based on previous studies [45–47] and were used to monitor the stress distribution within the reinforced layers.

Commercial displacement sensors with a 150 mm stroke measured the surface deformation during the test, while an S-type load cell with a capacity of 50 kN was employed to measure the loads applied by the actuator.

Each test section was instrumented with three total stress cells embedded within the subgrade, two surface displacement sensors, and one S-type load cell positioned along the loading axis of the hydraulic actuator. This configuration enabled the simultaneous recording of stress distribution, surface deformation, and applied load throughout the cyclic loading process, ensuring accurate data acquisition and correlation between mechanical response and loading conditions. Figure 5 shows the geometric configuration of the instrumentation within the test chamber.

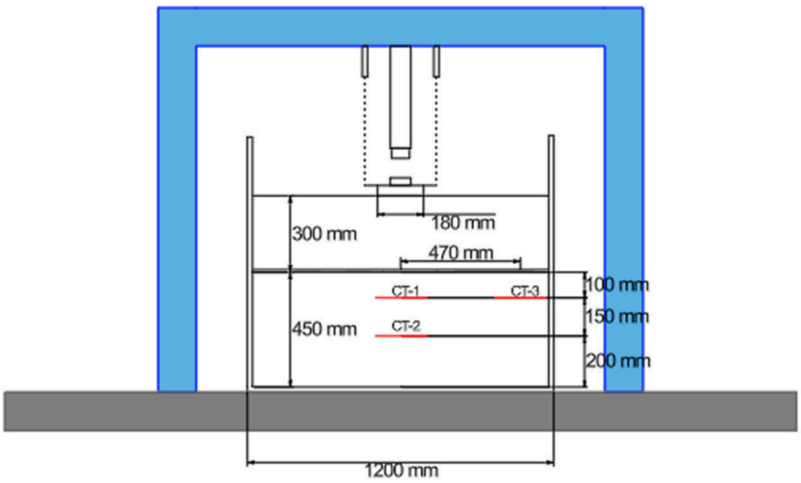


Figure 5. Location of Load cells.

To simultaneously capture the vertical stress gradient beneath the loading footprint and the lateral attenuation at a constant depth, two total stress cells (CT-1 and CT-2) were installed along the actuator's load axis, separated vertically by Δz = 15 mm. A third cell (CT-3) was positioned laterally at Δx = 43 cm to the right of the axis, at the same depth as CT-1, to measure the off-axis stress field and serve as a reference for the stress redistribution induced by the reinforcement.

The two displacement potentiometers were positioned on the surface, aligned with the edge of the loading plate and spaced by the plate diameter (180 mm), to capture the local vertical deformation at the extreme points of load application. Finally, the load cell was mounted coaxially with the actuator.

Data Acquisition

Data acquisition and processing were performed using a National Instruments data acquisition card, connected to a LabVIEW V. 2015-based software interface. This setup automated the real-time recording of displacements, stresses, and loads throughout the cyclic loading tests.

2.3.3. Test Assembly

The assembly of the tests was carried out using a controlled sequence of activities, ensuring uniformity in the construction of each section and reliability in the instrumental records.

Step 1. Subgrade Preparation

The subgrade was constructed in layers approximately 150 mm thick and compacted to 80% of the maximum Modified Proctor density. This compaction level was intentionally selected to simulate weak support conditions representative of low-volume tertiary roads. Compaction control followed INVÍAS procedures [32], which are methodologically comparable to ASTM D155-12 (2021) [48]. The moisture content during compaction was maintained within $\pm$2% of the optimum moisture content. In situ density and moisture checks were performed on each layer to ensure uniform conditions throughout the specimen.

Localized excavations were performed at the designated instrumentation points, on which a 20 mm thick bed of sand was placed, leveled, and lightly compacted to provide uniform support for the stress cells. The subgrade material was placed, ensuring a minimum cover of 100 mm above each cell to guarantee stability and to minimize stress concentration effects. This procedure follows the methodology proposed [49] for stress cell placement in granular materials. All load cells were calibrated under the same conditions.

Step 2. Installation of the Reinforcement (Geocells)

The geocells, both commercial and made from recycled tires, were installed according to the experimental configuration of each test. The support surface was previously leveled and compacted to ensure continuity in the transmission of forces. The cells were deployed and fixed in position, verifying their geometric alignment before filling.

The geocells were filled in successive layers of 100–150 mm, using granular material (fill or base material). Each layer was compacted with the selected equipment until the density and moisture parameters established in the laboratory were achieved, minimizing discontinuities and ensuring adequate confinement of the material within the cells, as shown in Figure 6.

Step 3. Construction of the Granular Base Layer

Once the geocells were installed, the granular base layer was placed on the compacted surface. The material was spread in controlled layers of 150 mm and compacted to 95% of the maximum Modified Proctor density, with uniformity verified at each stage through in situ density and moisture tests. This process ensured proper interaction between the

granular material and the reinforcement, as well as the structural stability of the test section, as shown in Figure 7.



Figure 6. (**a**) Subgrade preparation and compaction, (**b**) Geocell installation and alignment, and (**c**) Filling and compaction of granular material in geocells.



Figure 7. Granular base layer construction.

Step 4. Loading System and Surface Instrumentation

The circular plate with a diameter of 180 mm was installed on the compacted surface of the base, ensuring uniform contact with the granular material.

Surface displacement sensors were positioned at predefined locations to record deformations at two extreme points and to calculate the average surface deflection. Finally, the S-type load cell was installed coaxially with the hydraulic actuator, enabling simultaneous measurement of the applied load and the resulting deformation during each loading cycle.

To minimize edge effects, the inner walls of the chamber were kept smooth and lubricated, promoting a uniform stress distribution. This assembly sequence ensured the repeatability of the tests and the reliability of the measurements, providing experimental conditions consistent with those reported in previous studies [50–54].

2.4. Performance Evaluation and Analysis

The performance of the test sections was evaluated based on deformation response and degradation of the granular material. Key performance indicators were used to quantify the mechanical behavior of the reinforced and unreinforced configurations.

2.4.1. Breakage Index Bg %

The degradation of the granular material was evaluated using the breakage index (Bg), defined by [55], which expresses the percentage by weight of fractured particles. The calculation is based on comparing the material retained in each sieve before and after each test, considering only positive differences. The samples were carefully collected just below the load transfer plate, in the structural layer, at the end of the loading stage under initial conditions and before the maintenance stage. This procedure allowed the mechanical stability of the aggregates to be assessed and the influence of geocell confinement on the reduction in particle crushing to be analyzed.

2.4.2. Traffic Benefit Ratio

The Traffic Benefit Ratio (TBR) was used to evaluate the structural efficiency of geocells made from recycled tires as reinforcement in the experimental test. According to [56], this index is defined as the ratio between the cumulative number of load cycles required to reach a limit state of deformation in a reinforced section and the corresponding number in an unreinforced section, keeping the pavement geometry and material properties constant. The TBR is calculated using the following expression:

$$TBR = \frac{N_r}{Nu} \tag{1}$$

where

N_r: Number of load cycles that the reinforced section can withstand before reaching the limit deformation.

Nu: Number of load cycles that the cross-section without reinforcement can withstand before reaching the limit deformation.

In this study, a value of 75 mm was established as the limit deformation to ensure comparability between the different configurations, following the criteria used in the literature. Studies such as [21,57–60] have used this index to quantify the structural benefits of including geocells in pavement layers.

2.4.3. Flexibility Index

Another tool used to compare and evaluate the efficiency of reinforcement configurations in tertiary roads, especially in the early stages of cyclic loading, is the Flexibility Index (FI). This index aims to quantify the system's ability to adapt to progressive deformations under repeated loads without compromising its structural integrity. The calculation of the FI is based on the cumulative deformation rate (v, mm/cycle), measured in the initial stages of loading, taking the third cycle as a reference.

The choice of this cycle is supported by previous studies [22,61], which highlights that the first cycles are decisive for evaluating the initial mechanical response of the tracks. FI is defined by the following expression:

$$FI : 1 - \frac{v_{Reinforced}}{v_{Unreinforced}} \tag{2}$$

where

$v_{Reinforced}$: Cumulative deformation rate at cycle 3 for the reinforced section (mm/cycle).

$v_{Unreinforced}$: Cumulative deformation rate at cycle 3 for the unreinforced section (mm/cycle).

FI is interpreted as a value between 0 and 1, where 0 indicates that the reinforcement had no effect and values close to 1 reflect a significant reduction in initial deformation, thus demonstrating the greater effectiveness of the reinforcement. This procedure was applied systematically to all experimental configurations, both with a granular base and local backfill, constituting a standardized comparative parameter for classifying the structural performance of reinforced sections under repeated loads.

3. Results and Discussion

3.1. Deformation Response of Geocell-Reinforced Systems Under Cyclic Loading

The accumulation of vertical surface displacement under cyclic loading reflects the confinement efficiency of the geocell material and its ability to redistribute stresses within the granular layer.

3.1.1. General Evaluation of Accumulated Displacement Before Maintenance

Figure 8 illustrates the relationship between load cycles and accumulated surface deformation for the recebo infill configurations. The unreinforced section (UNR) reached failure before 25,000 cycles, with cumulative displacements slightly exceeding 290 mm, indicating a limited capacity of the unconfined granular layer to sustain repeated loading.

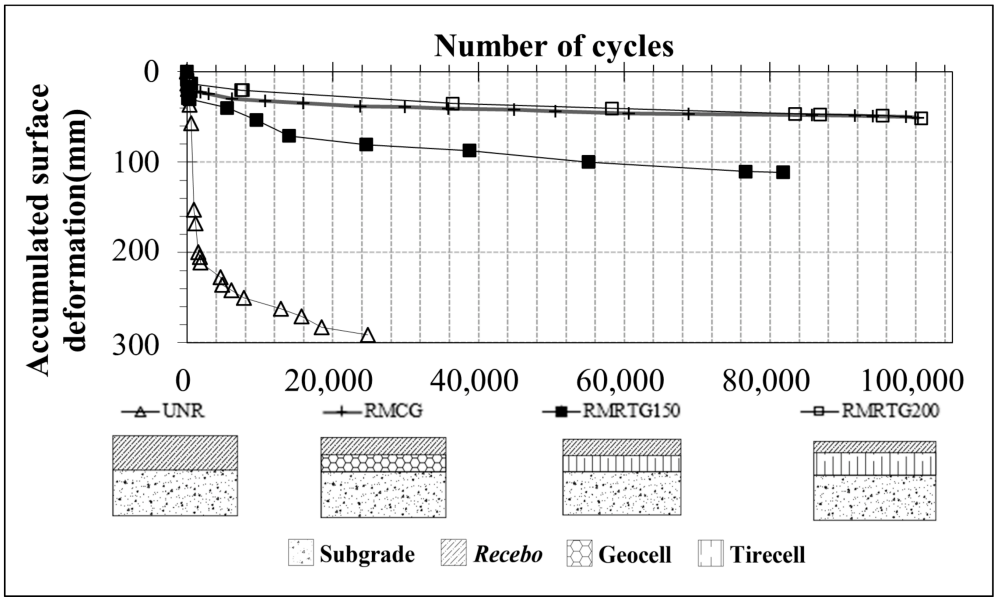


Figure 8. Accumulated surface deformations for the initial phase with recebo material.

In contrast, all reinforced configurations exhibited a pronounced reduction in deformation and a substantial increase in load-bearing capacity, confirming the effectiveness of geocell confinement. The RMRTG150 configuration reached accumulated displacements close to 110 mm and sustained more than 80,000 cycles, corresponding to a significant improvement relative to the unreinforced condition. However, both RMRTG200 and RMCG configurations exhibited markedly enhanced performance, reaching accumulated displacements of approximately 50 mm while maintaining stable responses beyond 100,000 cycles.

When compared to the unreinforced section, RMRTG150 achieved a 62% reduction in accumulated surface deformation, while RMRTG200 and RMCG reached reductions of 82% and 83%, respectively. The similar performance of RMRTG200 and RMCG suggests that cell height is a dominant factor influencing confinement efficiency under the tested

conditions. However, it should be noted that these two configurations differ not only in wall material but also in cell height, cell geometry, and connection method. Therefore, the observed performance differences should be interpreted as representative of the specific geocell systems evaluated rather than as an isolated effect of the wall material.

The small difference in accumulated displacement (0.55 mm), together with the higher number of load cycles sustained by RMRTG200, suggests variations in the confinement behavior of the recycled tire-based system under the tested conditions. However, further material characterization is needed to better understand the underlying mechanisms governing this response.

In contrast, the lower performance of RMRTG150 confirms that insufficient confinement height limits the effectiveness of the reinforcement, regardless of material type.

For the base material (Figure 9), similar trends were observed, although with a more pronounced contrast between reinforced and unreinforced conditions. The UNR configuration failed before 2000 cycles.

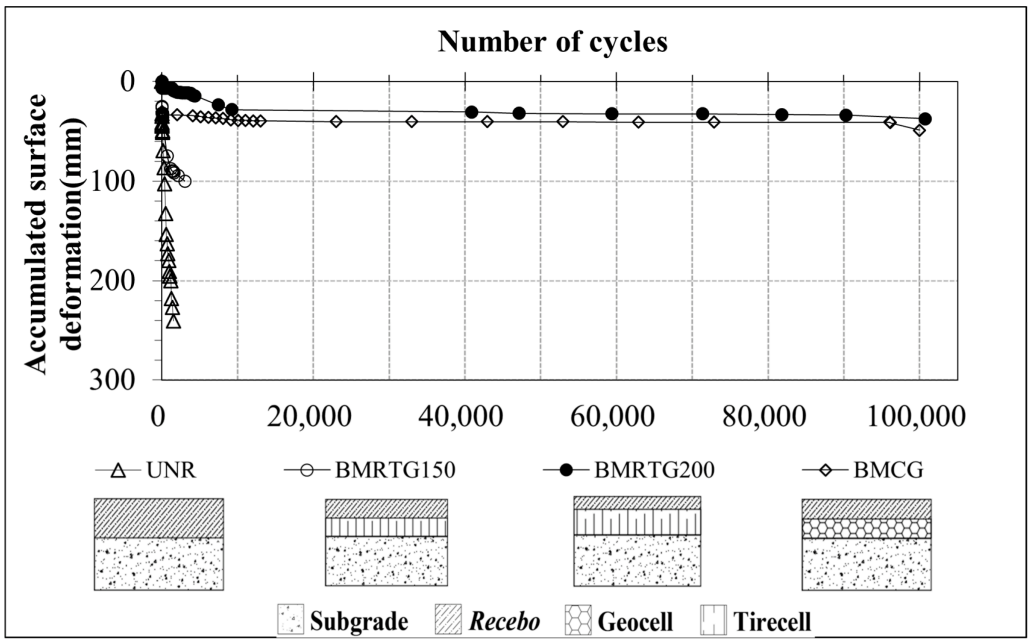


Figure 9. Accumulated surface deformations for the initial phase with base material.

Both BMRTG200 and BMCG completed the full 100,000-cycle loading program, with accumulated displacements of approximately 38 mm and 49 mm, corresponding to reductions of 84.2% and 79.6%, respectively. BMRTG200 exhibited slightly lower deformation than the commercial geocell, with a difference of 11 mm and 728 additional load cycles, suggesting a positive contribution of the rubber material to long-term deformation control under high-quality infill conditions.

In contrast, BMRTG150 showed significantly higher deformations, reaching values 2.6 times greater than BMRTG200 and 2.0 times greater than BMCG, confirming that reduced cell height limits confinement efficiency.

Overall, the pre-maintenance results confirm that all reinforced configurations outperformed the unreinforced sections for both infill materials. The 200 mm recycled tire geocell achieved deformation control and load endurance comparable to, and in some cases slightly exceeding, the commercial HDPE system. These results indicate that properly dimensioned recycled rubber geocells represent a technically viable alternative, with cell height governing confinement efficiency and overall structural response under cyclic loading.

3.1.2. General Evaluation of Accumulated Displacements After Maintenance

Following surface reconditioning and recompaction, all configurations exhibited reduced absolute deformation levels compared to the initial phase, while the relative performance hierarchy among configurations remained fully consistent with the pre-maintenance results. This consistency indicates that the confinement mechanism provided by the geocell wall material is preserved after surface intervention, regardless of infill type.

Figure 10 shows the accumulated surface deformation after maintenance for the recebo configurations. The unreinforced section (UNR-MNT) failed before 25,000 load cycles, with accumulated displacement exceeding 120 mm, indicating that maintenance improves short-term response but does not ensure stability under repeated loading in the absence of lateral confinement. All reinforced configurations exhibited stable responses throughout the test duration. RMRTG150-MNT reached deformations close to 60 mm after 100,000 cycles, whereas both RMRTG200-MNT and RMCG-MNT reached approximately 35 mm under the same loading conditions, with a difference of only 1.1%. These results confirm that maintenance does not alter the relative performance hierarchy and that recycled tire geocells with sufficient height maintain confinement efficiency comparable to that of the commercial system after intervention.

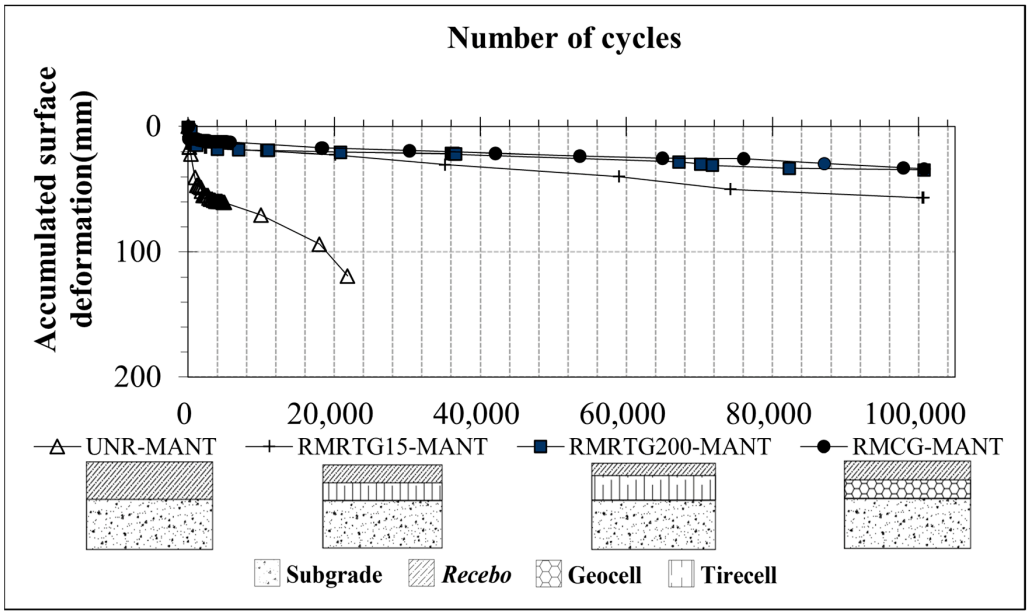


Figure 10. Post-maintenance accumulated surface deformation using recebo material.

Figure 11 presents the post-maintenance response for the base material configurations. The UNR-MNT section failed before 7600 cycles, with accumulated displacement exceeding 75 mm. BMRTG150-MNT reached deformations close to 45 mm after 103,700 cycles, while BMRTG200-MNT recorded approximately 34 mm after 100,730 cycles and RMCG-MNT approximately 43 mm after 104,281 cycles. Under comparable loading conditions, BMRTG200-MNT exhibited the lowest accumulated surface deformation, approximately 21% lower than the commercial geocell section, whereas BMRTG150-MNT showed deformations about 32% higher than BMRTG200-MNT. These results confirm that surface reconditioning reduces absolute deformation levels without altering the relative performance of the configurations, and that the lateral confinement capacity of properly dimensioned recycled tire geocells is preserved after maintenance operations.

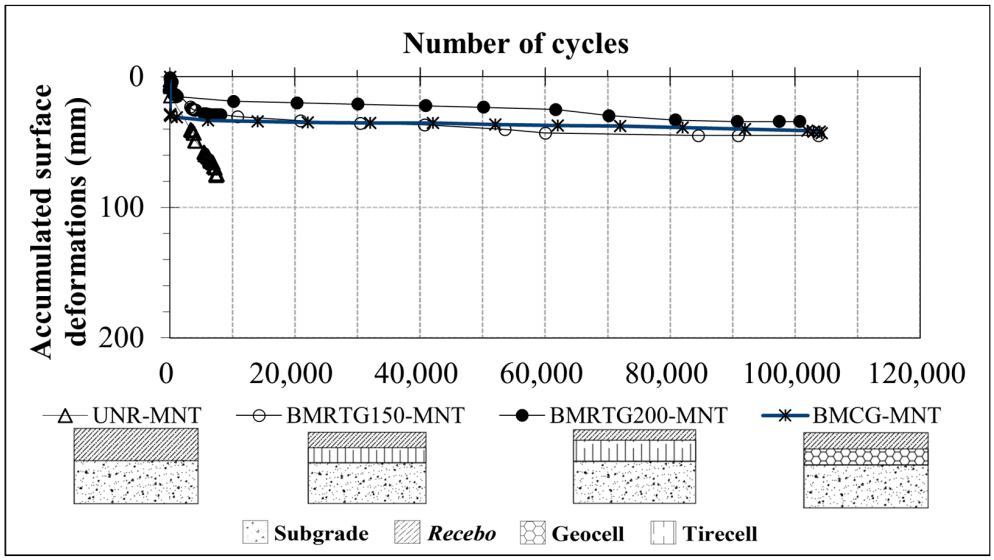


Figure 11. Post-maintenance accumulated surface deformations using base material.

The consistent performance observed across both infill materials indicates that confinement efficiency is preserved after maintenance, with RMRTG200-MNT exhibiting a response nearly identical to RMCG-MNT under recebo conditions and improved performance under base material. This behavior demonstrates the capacity of the recycled tire geocell system to sustain its confinement response under repeated loading within the loading window evaluated. The results further support its potential applicability in scenarios where periodic maintenance may be required.

3.2. Traffic Benefit Ratio Evaluation

The TBR quantifies the improvement in load-bearing capacity provided by the geocell reinforcement system by relating the number of load cycles required to reach a 40 mm deformation threshold in reinforced and unreinforced sections. For configurations that did not reach 40 mm prior to test termination, the total number of cycles completed at the end of the loading program was considered for comparative interpretation. This distinction is relevant when interpreting TBR values among configurations with substantially different loading histories.

For the recebo material, the unreinforced section (UNR) was used as the reference condition with a TBR value of 1.0, as shown in Table 5. The RMRTG150 configuration achieved a TBR of 14.32, while RMCG reached 93.02. The RMRTG200 configuration recorded the highest TBR value, 151.33. These values should be interpreted comparatively, since the premature failure of the reference section strongly influences the magnitude of the ratio. Nevertheless, the results show a progressive increase in TBR with increasing cell height under the evaluated conditions.

Table 5. Evaluation of the TBR under load cycles with recebo material.

Test	N_r * (Cycles)	N_u (Cycles)	TBR
UNR	385.00	385.00	1
RMRTG150	5514.00	385.00	14.32
RMRTG200	58,263.00	385.00	151.33
RMCG	35,813.00	385.00	93.02

* Nr represents the number of load cycles required to reach the 40 mm deformation threshold, used for the calculation of the TBR. The total cycles and accumulated surface deformation at the end of the test are reported separately in Section 3.1.

Table 6 presents the results for the base material, showing a more pronounced contrast between reinforced and unreinforced conditions. The UNR section failed after only 30 cycles (TBR = 1.0), highlighting the high sensitivity of unconfined granular base layers to cyclic loading. Both BMRTG200 and BMCG sustained the full loading program, yielding TBR values of 3357.6 and 3202.83, respectively. The BMRTG200 configuration achieved a TBR approximately 5% higher than BMCG, indicating comparable or slightly superior structural efficiency.

Table 6. Evaluation of the TBR under load cycles with base material.

Test	N_r * (Cycles)	N_u (Cycles)	TBR
UNR	30	30	1
BMRTG150	100	30	3.33
BMRTG200	100,728	30	3357.6
BMCG	96,085	30	3202.83

* Nr represents the number of load cycles required to reach the 40 mm deformation threshold, used for the calculation of the TBR. The total cycles and accumulated surface deformation at the end of the test are reported separately in Section 3.1.

The difference becomes more pronounced when compared with BMRTG150, which recorded a TBR of only 3.33, nearly three orders of magnitude lower than the 200 mm configurations. This significant disparity demonstrates that insufficient confinement height leads to rapid structural degradation, regardless of the material used. In contrast, adequate cell height enables effective load transfer and prevents early failure by maintaining lateral confinement within the granular matrix. It should be noted, however, that the exceptionally high TBR values recorded for the base material configurations reflect the early failure of the unreinforced section under laboratory conditions, and should therefore be interpreted as indicators of relative structural improvement rather than absolute field performance predictors.

Previous studies have reported significant improvements in load-bearing capacity due to geocell confinement [62,63]. However, the magnitude of the TBR values observed, particularly for the 200 mm configurations, highlights the dominant role of cell geometry in governing structural performance under cyclic loading. Furthermore, the comparable or improved response of recycled tire geocells supports their viability as a sustainable alternative, capable of achieving equivalent mechanical performance to conventional systems while contributing to material circularity [64,65].

3.3. Breakage Index

The breakage index (Bg) quantifies the granulometric variation induced by cyclic loading and provides insight into stress transfer mechanisms at the aggregate contact level. Due to the contrasting mechanical properties of recycled rubber and HDPE, differences in stress concentration and energy dissipation have been proposed in the literature; however, these mechanisms were not directly measured in this study. The Bg results are therefore interpreted in terms of observed aggregate response rather than confirmed material-level mechanisms.

3.3.1. Breakage Index of Base Type Material

For the base material, Bg values show clear differences among configurations (Figure 12). The unreinforced section (UNR) recorded 12.51%, while BMRTG150 reached 15.69%, BMCG 23.33%, and BMRTG200 the highest value at 30.86%.

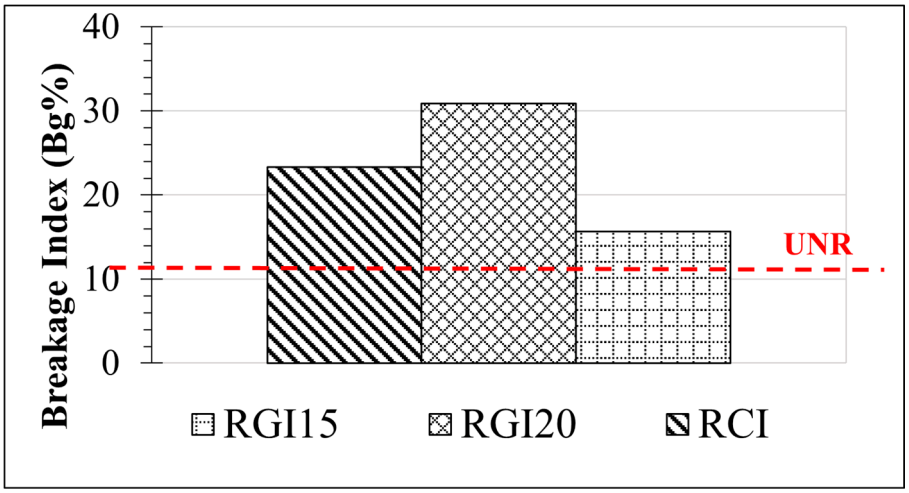


Figure 12. Breakage index for base material. Bg values (%) for UNR, BMRTG150, BMCG, and BMRTG200 configurations.

These results suggest that geocell height plays an important role in the stress state developed within the granular matrix under the tested conditions. The higher Bg observed in BMRTG200 reflects increased normal stresses at particle contacts due to enhanced lateral confinement, whereas the lower values in BMRTG150 indicate a limited ability to mobilize confinement under cyclic loading. Because the reinforced sections sustained a much greater number of load cycles than the unreinforced section, they experienced substantially higher cumulative cyclic loading exposure. Therefore, the interpretation of final Bg values should account for this difference in loading history.

Although the base material exhibited lower Bg values overall, greater particle breakage was observed in the reinforced configurations. This trend coincided with the substantially higher number of load cycles sustained by the reinforced sections. For example, BMRTG200 completed more than 100,000 cycles, whereas the unreinforced section (UNR) failed before 2000 cycles. Therefore, the higher Bg values should be interpreted in the context of the different cumulative loading exposure experienced by each configuration, rather than as an isolated indicator of poorer structural performance. Nevertheless, the relationship between particle breakage and long-term structural response requires further investigation.

3.3.2. Breakage Index of Recebo-Type Material

For the recebo material, Bg values also varied significantly among configurations (Figure 13). The unreinforced section (UNR) recorded a Bg value of 30.98%, RMRTG150 showed 30.53%, RMRTG200 reached 39.16%, and RMCG exhibited the highest fragmentation at 43.39%. As observed for the base material, the final Bg values should be interpreted with caution because the configurations were subjected to markedly different cumulative loading histories.

A comparison between commercial and recycled tire geocells showed greater particle breakage in the HDPE geocell configuration, whereas the recycled tire configurations, particularly RMRTG150, exhibited lower Bg values. However, since these systems differ not only in wall material but also in cell height, geometry, and connection method, the observed differences in Bg cannot be attributed exclusively to the rubber material. The lower Bg values may reflect the combined influence of confinement geometry and system response within the confined aggregate. However, the individual contribution of each variable, particularly the role of material properties in stress concentration, was not directly evaluated in the present study and requires further investigation.

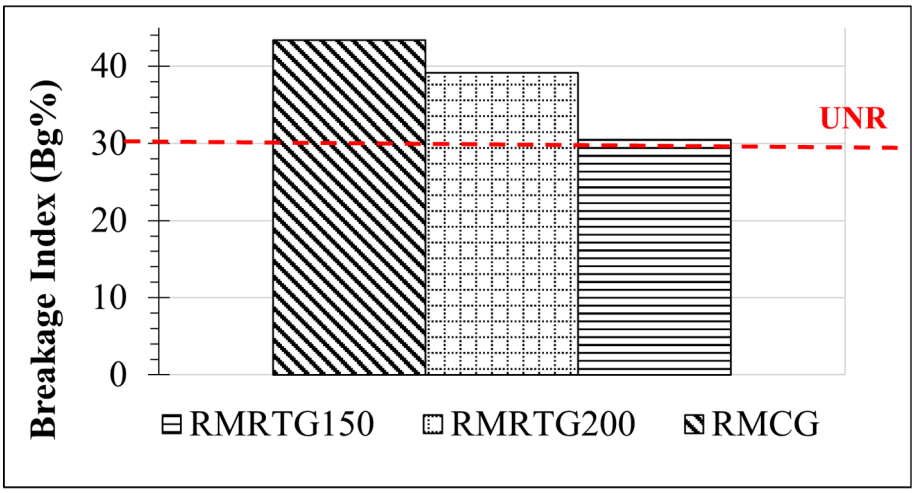


Figure 13. Breakage index for recebo material. Bg values (%) for UNR, RMRTG150, RMRTG200, and RMCG configurations.

The higher Bg observed in RMRTG200, compared to RMRTG150, is consistent with increased confinement, which enhances load transfer but also raises contact stresses between particles. This reflects a trade-off between structural performance and aggregate degradation, where improved confinement leads to greater load endurance at the expense of increased particle interaction and breakage.

Overall, the results indicate that susceptibility to particle fragmentation is strongly influenced by the type of infill material, with recebo showing higher degradation levels across all configurations. Several values exceeded the 28% reference threshold, suggesting potential limitations for applications under higher traffic conditions.

In contrast, the base material exhibited lower Bg values, indicating improved resistance to long-term degradation. These findings demonstrate that aggregate durability is governed not only by geocell geometry but also by infill material properties and stress transfer mechanisms. While increased confinement enhances structural performance, the use of recycled rubber contributes to reducing localized stress concentrations, improving the balance between load-bearing capacity and material degradation.

3.4. System Flexibility Analysis

The Flexibility Index (FI), calculated from the cumulative deformation rate at cycle 3, characterizes the early-stage mobilization of confinement and reflects the immediate mechanical response of the reinforced system under loading. This parameter is particularly useful for evaluating how quickly the geocell system activates its confinement mechanism, providing insight into initial deformation control prior to long-term stabilization.

3.4.1. Analysis of System Flexibility with Recebo-Type Material

Figure 14 presents the FI results for the recebo material. The unreinforced configuration (UNR) shows values close to zero, indicating a limited capacity to control deformation during the early loading stage. In contrast, all reinforced configurations exhibit positive FI values, reflecting the contribution of lateral confinement in reducing the initial rate of deformation.

The RMRTG150, RMRTG200, and RMCG configurations show comparable FI values, ranging approximately between 0.55 and 0.70. RMRTG200 achieved the highest value, exceeding the others by around 10–15%, which indicates a slightly more efficient mobilization of confinement during the initial loading cycles. These results suggest that, under recebo conditions, early-stage response is primarily governed by geocell geometry rather than

wall material. This trend is consistent with the deformation and TBR results, where the 200 mm configurations exhibited superior overall performance.

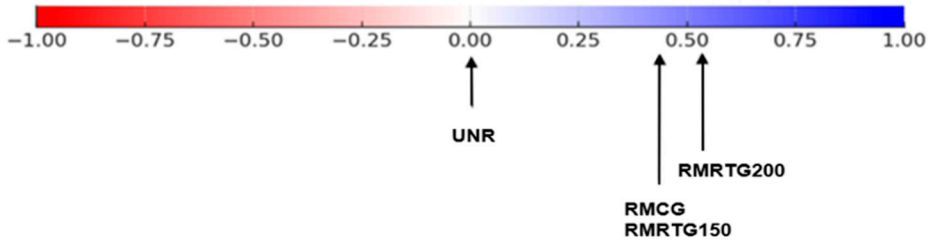


Figure 14. Flexibility Index (FI) comparative performance diagram for configurations with recebo material. FI values are shown for UNR, RMRTG150, RMRTG200, and RMCG configurations at cycle 3.

3.4.2. Analysis of System Flexibility with Base-Type Material

The results obtained for the base material are shown in Figure 15. The UNR and BMRTG150 configurations exhibit values close to zero, indicating limited improvement in early-stage deformation control. In contrast, BMCG and BMRTG200 show significantly higher FI values, ranging approximately between 0.50–0.60 and 0.75–0.90, respectively.

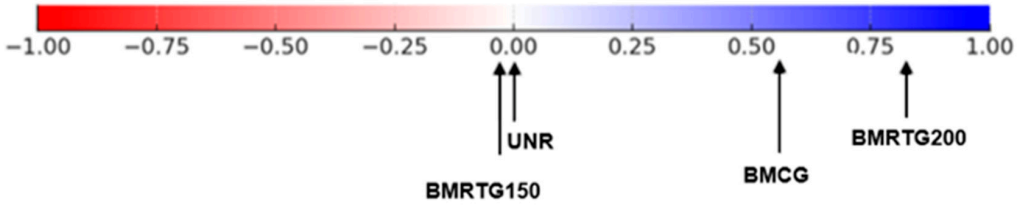


Figure 15. Flexibility Index (FI) comparative performance diagram for configurations with base-type material. FI values are shown for UNR, BMRTG150, BMCG, and BMRTG200 configurations at cycle 3.

BMRTG200 achieved the highest FI, exceeding the commercial geocell by approximately 30–50%, suggesting a more efficient early mobilization of lateral confinement under the tested conditions. This behavior is consistent with cell height playing a stronger role in the rate of confinement activation. However, the specific material-level mechanisms, including energy dissipation, were not directly measured in this study and require dedicated material characterization in future work before they can be confirmed. Conversely, the low FI of BMRTG150 suggests insufficient lateral restraint during the initial cycles, which is consistent with its lower TBR and higher accumulated surface deformation.

3.5. Evaluation of Total Stresses

This section summarizes the total stresses measured within the subgrade of the physical models. Three load cells were installed: Load Cell B directly beneath the applied load, Load Cell A at a depth of 150 mm below B, and Load Cell C near the lateral boundary. This configuration allows evaluation of both vertical stress transmission and lateral redistribution within the system.

3.5.1. Total Stresses: Base-Type Material

The stress measurements for the base material show a consistent distribution pattern. Load Cell B recorded the highest stresses, followed by Load Cell A, while Load Cell C registered the lowest values, reflecting the expected stress gradient beneath a surface load.

Figure 16 presents the stress distribution for the unreinforced condition (UNR). The highest stresses were concentrated beneath the load, reaching approximately 669 kPa at point B, while point A recorded about 380 kPa and point C approximately 211 kPa. This distribution indicates limited stress dissipation in the absence of confinement.

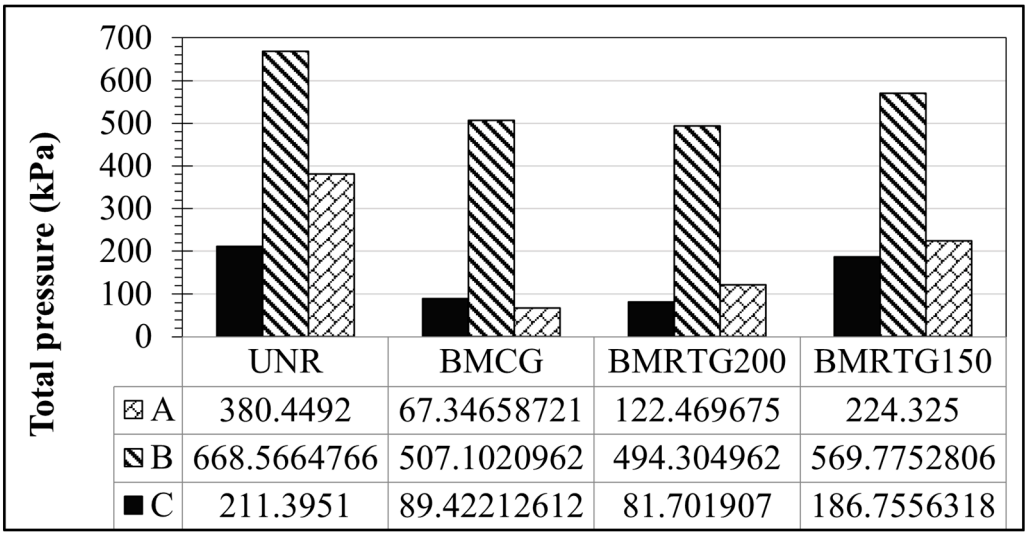


Figure 16. Total stresses with base material. Stress values (kPa) at load cells A, B, and C for UNR, BMCG, BMRTG200, and BMRTG150 configurations.

In contrast, all reinforced configurations modified the stress transmission mechanism. Stresses measured at deeper (A) and lateral (C) locations were reduced, indicating that part of the applied load was redistributed within the reinforced layer. This behavior reflects the development of a load-spreading response, where the geocell-confined layer acts as a semi-rigid slab that distributes stresses before transferring them downward.

The concentration of stresses at Load Cell B in reinforced sections should not be interpreted as detrimental. Instead, it confirms that the reinforced layer absorbs and redistributes loads, reducing stress propagation to underlying layers. This mechanism is consistent with the lower accumulated surface deformations and higher TBR values observed for reinforced configurations.

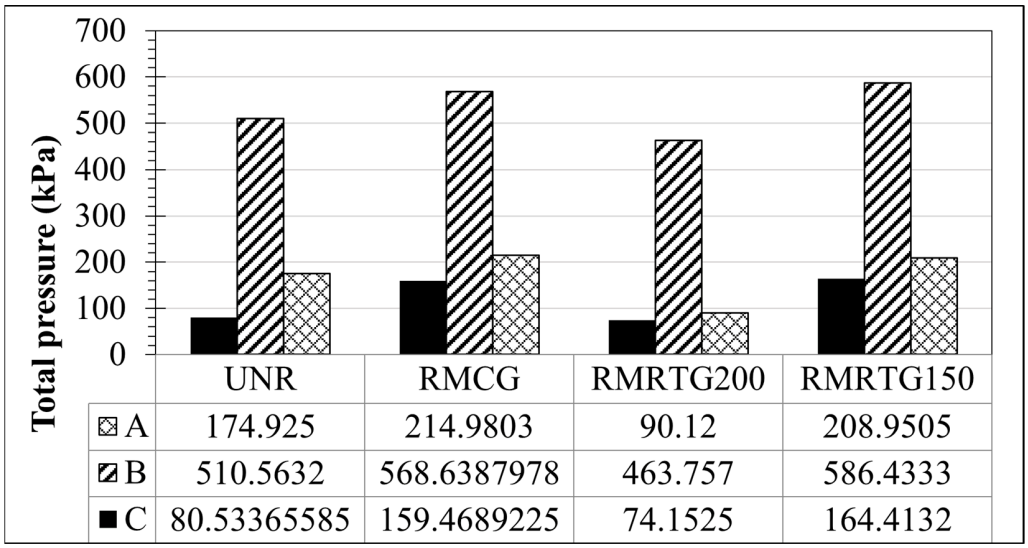
Among the reinforced systems, BMRTG200 exhibited the most efficient stress redistribution, reducing stresses at both A and C compared to BMRTG150. The commercial geocell showed a similar trend, although with slightly higher stress transmission. These results confirm that cell height plays a dominant role in controlling stress distribution within the system.

3.5.2. Total Stresses: Recebo Material

Figure 17 presents the stress distribution for the recebo material. In the unreinforced condition, stresses were again concentrated beneath the load, reaching approximately 511 kPa at point B, while point A recorded about 175 kPa and point C approximately 81 kPa.

Reinforced configurations significantly altered this distribution. The RMRTG200 configuration exhibited the most favorable response, with lower stresses at both A and C and a more uniform stress distribution across the system. In contrast, RMRTG150 showed higher stress concentrations, indicating less effective load redistribution. The commercial geocell exhibited intermediate behavior.

The reduced stresses measured at deeper and lateral positions confirm that geocell reinforcement enhances load-spreading within the granular layer. This effect limits the transmission of stresses to the subgrade, contributing to lower surface deformation and improved structural performance, as reflected in the TBR and deformation results.



	UNR	RMCG	RMRTG200	RMRTG150
A	174.925	214.9803	90.12	208.9505
B	510.5632	568.6387978	463.757	586.4333
C	80.53365585	159.4689225	74.1525	164.4132

Figure 17. Total stresses with recebo material. Stress values (kPa) at load cells A, B, and C for UNR and reinforced configurations.

3.6. Circular-Economy and Life-Cycle Implications

Although this study does not include a full life cycle assessment (LCA), material flow analysis (MFA), or life cycle costing (LCC), the experimental results allow a preliminary discussion of the circular-economy implications of recycled tire geocells. For comparative discussion purposes, the reference basis adopted here is 1 m^2 of installed geocell reinforcement in an unpaved road section under the tested loading conditions. In this context, recycled tire geocells provide a direct valorization pathway for end-of-life tires by transforming tread sections into functional reinforcement elements without chemical processing. Based on the effective usable tread area after sidewall removal and cutting losses associated with fabrication, approximately 16 end-of-life tires are reused per square meter of installed geocell. For a reinforced road Section 3.5 m wide with a single geocell layer, this corresponds to approximately 56,000 end-of-life tires per kilometer. Compared with conventional HDPE geocells, this approach may reduce the demand for virgin polymeric materials while simultaneously contributing to waste diversion. In addition, the improved deformation control observed under cyclic loading suggests the potential for reduced maintenance demand in low-volume roads, although this should be confirmed through future field validation and life cycle costing studies. These environmental and resource-related implications should therefore be interpreted as preliminary, since they do not yet account for transport, labor requirements, durability variability, or end-of-life management, and require confirmation through dedicated LCA, MFA, and LCC analyses.

4. Conclusions

This study experimentally evaluated the cyclic response of recycled tire geocells used as confinement systems for unpaved road reinforcement through large-scale laboratory testing using two granular infill materials and comparison with a commercial HDPE geocell system. Based on the experimental results obtained under the tested conditions, the following conclusions are drawn.

The recycled tire geocell with 200 mm height (BMRTG200 and RMRTG200, depending on infill type) showed lower accumulated surface deformation and higher sustained loading cycles than the unreinforced sections under both granular infill conditions evaluated. Under the experimental configuration adopted in this study, RTG200 exhibited a response

comparable to the commercial HDPE geocell in several performance indicators, including accumulated surface deformation and loading endurance.

The experimental results indicate that geocell height influenced the measured reinforcement response. The 150 mm recycled tire geocell configurations (BMRTG150 and RMRTG150) generally exhibited lower performance than RTG200 in terms of accumulated surface deformation and load-carrying capacity within the loading range evaluated. These findings suggest that geometry should be considered as a relevant parameter when designing recycled tire geocell systems. It should be noted that the recycled tire and HDPE geocell configurations evaluated in this study also differed in cell height, geometry, and connection method; therefore, observed performance differences reflect the response of specific geocell systems and should not be attributed solely to the wall material.

Aggregate breakage results showed different fragmentation responses among the reinforced configurations. Higher breakage values were observed in some configurations subjected to larger numbers of loading cycles, indicating that aggregate degradation and reinforcement performance should be evaluated jointly when assessing reinforced granular systems.

The post-maintenance evaluation showed that the RTG200 configurations and the commercial geocell system (BMCG and RMCG) exhibited similar accumulated surface deformation responses after surface reconditioning under the loading conditions evaluated. These results indicate that the recycled tire geocell maintained its measured response following the maintenance procedure adopted in this study.

From a sustainability standpoint, the manufacturing process of tire-derived geocells requires no chemical transformation of the rubber, relying exclusively on mechanical cutting and staple assembly. Combined with the demonstrated structural performance, this positions recycled tire geocells as a viable pathway for the valorization of end-of-life tire waste within a circular economy framework, reducing reliance on virgin polymer in granular layer reinforcement applications.

The results presented in this study are strictly limited to the laboratory conditions, material properties, loading configuration, geocell geometries, and number of loading cycles evaluated. Single-specimen testing per configuration was adopted due to resource constraints, and no statistical replication was performed. This work does not address long-term creep effects, aging or environmental degradation, long-term confinement retention, or field-scale performance under real traffic and climate conditions. The proposed mechanisms related to energy dissipation and stress redistribution are inferred from structural observations and have not been confirmed through direct material characterization. Field validation under real traffic and subgrade variability conditions is required before design recommendations or large-scale implementation can be established. Additional studies incorporating mechanical characterization of recycled tire strips, durability assessment under environmental exposure, and extended loading programs are strongly recommended.

Author Contributions: M.P.S.: conceptualization, methodology, formal analysis, investigation, data curation, writing—original draft preparation, project administration. E.M.P.: conceptualization, validation, writing—review and editing, supervision. I.A.G.G.: validation, resources, writing—review and editing, supervision. K.Y.R.R.: writing—original draft preparation, visualization. J.S.P.D.: writing—original draft preparation, visualization., visualization. All authors have read and agreed to the published version of the manuscript.

Funding: This research received no external funding.

Data Availability Statement: The original contributions presented in this study are included in the article. Further inquiries can be directed to the corresponding author.

Acknowledgments: The authors gratefully acknowledge the support provided by the University of Ibagué, and the University of Brasília, during the development of this study, as well as the technical and academic contributions that made this research possible.

Conflicts of Interest: The authors declare no conflicts of interest.

Abbreviations

The following abbreviations are used in this manuscript:

HDPE	High-density polyethylene
UNR	Unreinforced section
BM	Base material
RM	Recebo material
CG	Commercial geocell
RTG	Recycled tire geocell
BMRTG150	Base material with recycled tire geocell, 150 mm height
BMRTG200	Base material with recycled tire geocell, 200 mm height
RMRTG150	Recebo material with recycled tire geocell, 150 mm height
RMRTG200	Recebo material with recycled tire geocell, 200 mm height
BMCG	Base material with commercial geocell
RMCG	Recebo material with commercial geocell
TBR	Traffic Benefit Ratio
Bg	Breakage index
FI	Flexibility Index
CBR	California Bearing Ratio
USCS	Unified Soil Classification System
INVIAS	Colombian National Roads Institute (*Instituto Nacional de Vías*)
SM	Silty sand
SW	Well-graded sand
GM-GW	Well-graded silty gravel
MNT	Post-maintenance condition
ASTM	American Society for Testing and Materials

References

1. Kirchherr, J.; Reike, D.; Hekkert, M. Conceptualizing the Circular Economy: An Analysis of 114 Definitions. *Resour. Conserv. Recycl.* **2017**, *127*, 221–232. [CrossRef]
2. Geyer, R.; Jambeck, J.R.; Law, K.L. Production, Use, and Fate of All Plastics Ever Made. *Sci. Adv.* **2017**, *3*, e1700782. [CrossRef] [PubMed]
3. Fazli, A.; Rodrigue, D. Recycling Waste Tires into Ground Tire Rubber (GTR)/Rubber Compounds: A Review. *J. Compos. Sci.* **2020**, *4*, 103. [CrossRef]
4. Thomas, B.S.; Gupta, R.C. A Comprehensive Review on the Applications of Waste Tire Rubber in Cement Concrete. *Renew. Sustain. Energy Rev.* **2016**, *54*, 1323–1333. [CrossRef]
5. Ambaye, T.G.; Djellabi, R.; Vaccari, M.; Prasad, S.; Aminabhavi, T.M.; Rtimi, S. Emerging Technologies and Sustainable Strategies for Municipal Solid Waste Valorization: Challenges of Circular Economy Implementation. *J. Clean. Prod.* **2023**, *423*, 138708. [CrossRef]
6. Yoon, Y.W.; Heo, S.B.; Kim, K.S. Geotechnical Performance of Waste Tires for Soil Reinforcement from Chamber Tests. *Geotext. Geomembr.* **2008**, *26*, 100–107. [CrossRef]
7. Siddique, R.; Naik, T.R. Properties of Concrete Containing Scrap-Tire Rubber—An Overview. *Waste Manag.* **2004**, *24*, 563–569. [CrossRef] [PubMed]
8. Hernández-Olivares, F.; Barluenga, G. Fire Performance of Recycled Rubber-Filled High-Strength Concrete. *Cem. Concr. Res.* **2004**, *34*, 109–117. [CrossRef]
9. Shu, X.; Huang, B. Recycling of Waste Tire Rubber in Asphalt and Portland Cement Concrete: An Overview. *Constr. Build. Mater.* **2014**, *67*, 217–224. [CrossRef]

10. Li, B.; Huang, M.; Zeng, X. Dynamic Behavior and Liquefaction Analysis of Recycled-Rubber Sand Mixtures. *J. Mater. Civ. Eng.* **2016**, *28*, 04016122. [CrossRef]
11. Adhikari, B. Reclamation and Recycling of Waste Rubber. *Prog. Polym. Sci.* **2000**, *25*, 909–948. [CrossRef]
12. Humphrey, D.N.; Katz, L.E. Water-Quality Effects of Tire Shreds Placed Above the Water Table: Five-Year Field Study. *Transp. Res. Rec. J. Transp. Res. Board* **2000**, *1714*, 18–24. [CrossRef]
13. Ahmed, I.; Lovell, C.W. *Transportation Research Record No. 1422—Lightweight Artificial and Waste Materials for Embankments over Soft Soils*; National Academy Press: Washington, DC, USA, 1993.
14. Edil, T.; Bosscher, P. Engineering Properties of Tire Chips and Soil Mixtures. *Geotech. Test. J.* **1994**, *17*, 453–464. [CrossRef]
15. Rajagopal, K.; Krishnaswamy, N.R.; Madhavi Latha, G. Behaviour of Sand Confined with Single and Multiple Geocells. *Geotext. Geomembr.* **1999**, *17*, 171–184. [CrossRef]
16. Dash, S.K.; Rajagopal, K.; Krishnaswamy, N.R. Behaviour of Geocell-Reinforced Sand Beds under Strip Loading. *Can. Geotech. J.* **2007**, *44*, 905–916. [CrossRef]
17. Pokharel, S.K.; Han, J.; Leshchinsky, D.; Parsons, R.L.; Halahmi, I. Investigation of Factors Influencing Behavior of Single Geocell-Reinforced Bases under Static Loading. *Geotext. Geomembr.* **2010**, *28*, 570–578. [CrossRef]
18. Han, J.; Pokharel, S.K.; Yang, X.; Manandhar, C.; Leshchinsky, D.; Halahmi, I.; Parsons, R.L. Performance of Geocell-Reinforced RAP Bases over Weak Subgrade under Full-Scale Moving Wheel Loads. *J. Mater. Civ. Eng.* **2011**, *23*, 1525–1534. [CrossRef]
19. Chen, R.H.; Chiu, Y.M. Model Tests of Geocell Retaining Structures. *Geotext. Geomembr.* **2008**, *26*, 56–70. [CrossRef]
20. Madhavi Latha, G.; Rajagopal, K. Parametric Finite Element Analyses of Geocell-Supported Embankments. *Can. Geotech. J.* **2007**, *44*, 917–927. [CrossRef]
21. Pokharel, S.K.; Han, J.; Leshchinsky, D.; Parsons, R.L. Experimental Evaluation of Geocell-Reinforced Bases under Repeated Loading. *Int. J. Pavement Res. Technol.* **2018**, *11*, 114–127. [CrossRef]
22. Thakur, J.K.; Han, J.; Parsons, R.L. Factors Influencing Deformations of Geocell-Reinforced Recycled Asphalt Pavement Bases under Cyclic Loading. *J. Mater. Civ. Eng.* **2017**, *29*, 4016240. [CrossRef]
23. Bathurst, R.; Karpurapu, R. Large-Scale Triaxial Compression Testing of Geocell-Reinforced Granular Soils. *Geotech. Test. J.* **1993**, *16*, 296–303. [CrossRef]
24. Pening, J. *Inversión de Recursos Públicos en Infraestructura de Vías Terciarias*; Departamento Nacional de Planeación: Bogota, Colombia, 2023.
25. Mikou, M.; Rozenberg, J.; Koks, E.; Fox, C.; Quiros, T.P. *Assessing Rural Accessibility and Rural Roads Investment Needs Using Open Source Data Beyond the Gap Background Paper*; World Bank Group: Washington, DC, USA, 2019.
26. Biabani, M.M.; Indraratna, B.; Ngo, N.T. Modelling of Geocell-Reinforced Subballast Subjected to Cyclic Loading. *Geotext. Geomembr.* **2016**, *44*, 489–503. [CrossRef]
27. *INV E 102 13*; INVIAS Descripción e Identificación de Suelos. INVIAS: Bogota, Colombia, 2013.
28. *INV E-125*; Determinación Del Límite Líquido de Los Suelos. Instituto Nacional de Vías INVIAS: Bogota, Colombia, 2013.
29. *INV E 126-13*; Limite Plastico e Indice de Plasticidad de Los Suelos. INVIAS: Bogota, Colombia, 2013.
30. *INV E-128*; Determinación de La Gravedad Específica de Las Partículas Sólidas de Los Suelos y Del Llenante Mineral, Empleando Un Picnómetro Con Agua. Instituto Nacional de Vías INVIAS: Bogota, Colombia, 2013.
31. *INV E-148*; CBR de Suelos Compactados en El Laboratorio y Sobre Muestra Inalterada. Instituto Nacional de Vías INVIAS: Bogota, Colombia, 2013.
32. *INV E 142-13*; Relaciones de Humedad—Peso Unitario Seco en Suelos. INVIAS: Bogota, Colombia, 2013.
33. *INV E-181*; Sistema Unificado de Clasificación de Suelos Para Propósitos de Ingeniería. Instituto Nacional de Vías INVIAS: Bogota, Colombia, 2013.
34. *INV E-161*; Densidad y Peso Unitario Del Suelo en El Terreno Por El Método Del Cono y Arena. Instituto Nacional de Vías INVIAS: Bogota, Colombia, 2013.
35. *INV E-230*; Determinación Del Porcentaje de Terrones de Arcilla y Partículas Friables en Los Agregados. Instituto Nacional de Vías INVIAS: Bogota, Colombia, 2013.
36. *INV E-218*; Resistencia al Desgaste de Los Agregados de Tamaño Menor de 37.5 Mm (1 ½") Por Medio de La Máquina de Los Ángeles. Instituto Nacional de Vías INVIAS: Bogota, Colombia, 2013.
37. Sayao, A.; Gerscovich, D.; Medeiros, L.V.; Sieira, A.C.C.F. Scrap Tire-An Attractive Material for Gravity Retaining Walls and Soil Reinforcement. *J. Solid Waste Technol. Manag.* **2009**, *35*, 135–155. [CrossRef]
38. Susunaga, M.P.; Gongora, I.A.G.; Palmeira, E.M. Evaluation of the Impact of Sustainable Infrastructure on the Perception of the Community Through the Use of Geocells Made of Recycled Tires in an Educational Environment. *Sustainability* **2025**, *17*, 1791. [CrossRef]

39. Hidalgo Montoya, C.A.; Bustamante Hernández, J.J. SISTEMA DE REFUERZO DE SUELO CON LLANTAS EN DESUSO Y MÉTODO DE ELABORACIÓN DEL MISMO. Colombian Patent NC2017/0003522, 30 September 2018.
40. Qian, Y.; Han, J.; Pokharel, S.; Parsons, R. Performance of Triangular Aperture Geogrid-Reinforced Base Courses over Weak Subgrade under Cyclic Loading. *J. Mater. Civ. Eng.* **2013**, *25*, 1013–1021. [CrossRef]
41. Cancelli, A.; Montanelli, F.; Rimoldi, P.; Zhao, A. Full Scale Laboratory Testing on Geosynthetics Reinforced Paved Roads. In *Earth Reinforcement*; CRC Press: Boca Raton, FL, USA, 1996; Volume 1, pp. 573–578.
42. *ASTM D5311-22*; Standard Test Method for Load Controlled Cyclic Triaxial Strength of Stabilized Soils. ASTM International: West Conshohocken, PA, USA, 2022.
43. Palmeira, E.M.; Antunes, L.G.S. Large Scale Tests on Geosynthetic Reinforced Unpaved Roads Subjected to Surface Maintenance. *Geotext. Geomembr.* **2010**, *28*, 547–558. [CrossRef]
44. Leng, J.; Gabr, M.A. Characteristics of Geogrid-Reinforced Aggregate Under Cyclic Load. *Transp. Res. Rec.* **2002**, *1786*, 29–35. [CrossRef]
45. Palmeira, E.M.; Góngora, I.A.G. Assessing the Influence of Some Soil–Reinforcement Interaction Parameters on the Performance of a Low Fill on Compressible Subgrade. Part I: Fill Performance and Relevance of Interaction Parameters. *Int. J. Geosynth. Ground Eng.* **2015**, *2*, 1. [CrossRef]
46. Pires, A.C.G. Estudo Experimental do Comportamento de Tubos Enterrados em Solos Reforçados Com Geossinteticos. Ph.D. Thesis, Universidade de Basilia, Brasilia, Brazil, 2021.
47. Filho, J.M. Estudo da Interação Solo-Reforço Geossintético em Aterros Estaqueados por Meio de Ensaios de Grandes Dimensões. Ph.D. Thesis, Universidade de Brasilia, Brasilia, Brazil, 2022.
48. *ASTM D1557-12(2021)*; Standard Test Methods for Laboratory Compaction Characteristics of Soil Using Modified Effort (56,000 ft-lbf/ft^3 (2700 kN·m/m^3)). ASTM International: West Conshohocken, PA, USA, 2021.
49. Santos, E.C.G. Avaliação Experimental de Muros Reforçados Executados Com Resíduos de Construção e Demolição Reciclados (RCD-R) e Solo Fino. Doctoral Dissertation, Universidade de Brasília, Brasilia, Brazil, 2011.
50. Yin, Z.; Ndiema, K.M.; Lekalpure, R.L.; Kiptum, C.K. Numerical Study of Geotextile-Reinforced Flexible Pavement Overlying Low-Strength Subgrade. *Appl. Sci.* **2022**, *12*, 325. [CrossRef]
51. Gottumukkala, B.; Shaw, A.; Prasad, P.; Kamaraj, C. Laboratory Evaluation of a Geosynthetic-Reinforced Pavement over Poor Subgrade. In *International Conference on Civil Engineering Trends and Challenges for Sustainability*; Springer Nature: Singapore, 2023; pp. 443–455.
52. Arias, J.; Inti, S.; Tandon, V. Influence of Geocell Reinforcement on Bearing Capacity of Low-Volume Roads. *Transp. Dev. Econ.* **2020**, *6*, 5. [CrossRef]
53. Wright, J.; Kim, S.S.; Kim, B. Stiffness and Strength Improvement of Geosynthetic-Reinforced Pavement Foundation Using Large-Scale Wheel Test. *Infrastructures* **2020**, *5*, 33. [CrossRef]
54. Gottumukkala, B.; Mehar, B.; Minchala, D.; Pulikanti, S.; Kuna, K. Laboratory and Field Evaluations of Geocell Reinforced Bases for Locally Available Material in the Himalayan Region. *Int. J. Geosynth. Ground Eng.* **2023**, *9*, 74. [CrossRef]
55. Marsal, R.J. Large Scale Testing of Rockfill Materials. *J. Soil Mech. Found. Div.* **1967**, *93*, 27–43. [CrossRef]
56. Baadiga, R.; Balunaini, U.; Saride, S.; Madhav, M.R. Effect of Geogrid Type and Subgrade Strength on the Traffic Benefit Ratio of Flexible Pavements. *Transp. Infrastruct. Geotechnol.* **2023**, *10*, 180–210. [CrossRef]
57. Baadiga, R.; Balunaini, U.; Saride, S. PERFORMANCE OF REINFORCED BASE COURSES OF FLEXIBLE PAVEMENTS OVERLYING SOFT SUBGRADES: INSIGHTS FROM LARGE-SCALE MODEL EXPERIMENTS. *Int. J. GEOMATE* **2022**, *22*, 80–86. [CrossRef]
58. Saride, S.; Rayabharapu, V.K.; Vedpathak, S. Evaluation of Rutting Behaviour of Geocell Reinforced Sand Subgrades Under Repeated Loading. *Indian Geotech. J.* **2015**, *45*, 378–388. [CrossRef]
59. Önal, Y.; Çalışıcı, M.; Kayadelen, C.; Altay, G. A Comparative Experimental Study of Geocell and Geogrid-Reinforced Highway Base Layers under Repeated Loads. *Road Mater. Pavement Des.* **2023**, *24*, 2877–2892. [CrossRef]
60. Badiger, M.; Mamatha, K.H.; Dinesh, S.V. Evaluation of Commercial and Scrap Tyre Cellular Reinforcement Infilled with Demolition Waste for Granular Sub-Base of Flexible Pavements: A Sustainable Approach. *Int. J. Transp. Sci. Technol.* **2024**, *18*, 29–46. [CrossRef]
61. Moghaddas Tafreshi, S.N.; Dawson, A.R. A Comparison of Static and Cyclic Loading Responses of Foundations on Geocell-Reinforced Sand. *Geotext. Geomembr.* **2012**, *32*, 55–68. [CrossRef]
62. Imjai, T.; Pilakoutas, K.; Guadagnini, M. Performance of Geosynthetic-Reinforced Flexible Pavements in Full-Scale Field Trials. *Geotext. Geomembr.* **2019**, *47*, 217–229. [CrossRef]
63. Singh, M.; Trivedi, A.; Shukla, S.K. Evaluation of Geosynthetic Reinforcement in Unpaved Road Using Moving Wheel Load Test. *Geotext. Geomembr.* **2022**, *50*, 581–589. [CrossRef]

64. Khan, A.; Puppala, A.J.; Biswas, N.; Sarat Chandra Congress, S. Evaluation of the Structural Performance of the Geocell-Stabilized Flexible Pavement. *Transp. Geotech.* **2023**, *41*, 101021. [CrossRef]
65. Krishna, A.; Latha, G.M. Evolution of Geocells as Sustainable Support to Transportation Infrastructure. *Sustainability* **2023**, *15*, 11773. [CrossRef]

Disclaimer/Publisher's Note: The statements, opinions and data contained in all publications are solely those of the individual author(s) and contributor(s) and not of MDPI and/or the editor(s). MDPI and/or the editor(s) disclaim responsibility for any injury to people or property resulting from any ideas, methods, instructions or products referred to in the content.